International Journal of Nanomedicine

Dovepress
open access to scientific and medical research

Open Access Full Text Article

ORIGINAL RESEARCH

Regulating Preparation Of Functional Alginate-Chitosan Three-Dimensional Scaffold For Skin Tissue Engineering

This article was published in the following Dove Press journal:
International Journal of Nanomedicine

Tonghe Zhu[1]
Jia Jiang[1]
Jinzhong Zhao[1]
Sihao Chen[2,3]
Xiaoyu Yan[1]

[1]Department of Sports Medicine, Department of Orthopedics, Shanghai Jiao Tong University Affiliated Sixth People's Hospital, Shanghai 200233, People's Republic of China; [2]Scientific Research Department of Shanghai University of Engineering Science, Shanghai 201620, People's Republic of China; [3]Multidisciplinary Center for Advanced Materials of Shanghai University of Engineering Science, Shanghai University of Engineering Science, Shanghai 201620, People's Republic of China

Aim: In this study, we attempted to regulate the preparation of Alg-CS-Flu three-dimensional scaffolds via a facile freeze-drying method combined with amidation.

Materials and methods: Three-dimensional porous flurbiprofen-grafted alginate (Alg)–chitosan (CS) scaffolds were successfully prepared by a facile freeze-drying method combined with amidation for skin tissue engineering applications. Alg-CS composite was first used to load flurbiprofen (Flu), which is a kind of anti-inflammatory non-steroidal molecule. The Flu-loaded Alg/CS composite solution, through freeze-drying and 1-ethyl-3(3-(dimethylamino)propyl) carbodiimide/N-hydroxysuccinimide crosslinking to form an Alg-CS-Flu scaffold, exhibited a uniform and porous morphology that was characterized using scanning electron microscopy. The Alg-CS-Flu as-prepared scaffold was also characterized using Fourier-transform infrared spectroscopy, water contact angle, thermal properties, and stress-strain testing.

Results: The results reveal that Flu was successfully grafted onto the surfaces of the Alg-CS-Flu scaffold, which showed good hydrophilicity and appropriate mechanical properties. Furthermore, cell viability, cell morphology from cells cultured in vitro, and hematoxylin-eosin staining after the graft was subcutaneously embedded in mice for 7 d demonstrated that the Alg-CS-Flu scaffold had no unfavorable effects on the adhesion and proliferation of fibroblasts, as well as a good anti-inflammatory property.

Conclusion: The developed Alg-CS-Flu scaffold is proposed as a promising material or skin tissue engineering application.

Keywords: three-dimensional scaffold, flurbiprofen, freeze-drying, amidation, skin tissue engineering

Introduction

Skin tissue engineering is the scientific process of restoring the biological function of damaged tissues with the aid of compatible biomaterials.[1,2] An ideal skin tissue engineering material should have high liquid-absorbing capacity, proper gas permeation, biocompatibility, and antibacterial properties to protect the skin defect from infections, dehydration, and subsequent tissue damage.[3–6] During the past decade, a variety of biomaterials have been used for skin tissue repair, such as electrospun nanofibrous scaffolds, nanoparticles, sponges, hydrogels, and so on.[7–10] Among the many materials, natural biomedical materials have received extensive attention in skin tissue engineering due to their excellent biocompatibility properties. As one of the most attractive substances, chitosan (CS) has attracted wide attention due to its special properties, such as biodegradability, biocompatibility, nontoxicity, accelerated

Correspondence: Xiaoyu Yan
Department of Sports Medicine, Department of Orthopedics, Shanghai Jiao Tong University Affiliated Sixth People's Hospital, No. 600 Yishan Road, Shanghai 200233, People's Republic of China
Tel/Fax +86 21 24056088
Email xyyan@sjtu.edu.cn

submit your manuscript | www.dovepress.com
DovePress
http://doi.org/10.2147/IJN.S210329

wound healing, excellent sterilization properties, and the fact that it does not easily cause syneresis,[11–13] all of which makes chitosan-based materials suitable for a wide range of applications in skin tissue engineering. Alginate (Alg) is a natural polysaccharide polymer with a highly hydrophilic property extracted from algae or seaweed that is widely used as a thickener, coagulant, and dispersant in biomedical applications, especially in wound dressings.[14–16]

Flurbiprofen (Flu) is used as a kind of effective analgesic and anti-inflammatory active ingredient for surgical applications.[17,18] However, the single-dosage form with a long onset of action, weak drug effect, and a shorter duration of action limits its clinical application. Recently, much attention has been paid to the utilization of Flu in formulating pharmaceutically effective dosage forms.[19,20] Therefore, it has potential in biocomposites with various substances incorporated, such as CS and Alg.

Research on the preparation of composite materials by combining sodium alginate with biodegradable materials has become increasingly more widely used in tissue engineering scaffold preparations due to its anti-bacterial properties, easy functionalization, and non-irritating properties.[14,21,22] An epidermal-growth-factor-loaded CS composite porous scaffold was fabricated by Denkbas et al in combination with solvent evaporation and chemical crosslinking.[23] The results show that the CS scaffold has a sustained release effect on epidermal growth factor and can improve the effect of wound treatment. Zeng et al fabricated a fucoidan-modified chitosan/alginate (F-CS/Alg) scaffold to protect and control release of bFGF to regulate fibroblast migration activity.[24] The results show that the F43-CS/Alg scaffold exhibited a considerable elevation in cell viability and promoted L929 fibroblast migration efficiently and accelerated fibroblast migration for wound repair effectively. However, all of the above modification studies are based on the electrostatic interaction between the carboxyl group and primary amino group,[25] which will limit the grafting efficiency of functional factors.

In this study, we attempted to regulate the preparation of Alg-CS-Flu three-dimensional scaffolds via a facile freeze-drying method combined with amidation. The entire preparation strategy is described in Figure 1. First, Alg/CS composite solution was prepared via co-blending in solution. Second, the composite solution was freeze-dried to produce the porous scaffolds. Then, Alg and CS were crosslinked and numerous Flu molecules were grafted onto the surface of Alg-CS by amidation.

Materials And Methods

Materials

Flu (purity > 99%) was purchased from Shanghai Xinya Pharmaceutical Co., Ltd. (Shanghai, China). CS (medical grade, with a degree of deacetylation of 95% and a molecular weight of 1.5×10^5) and Alg (medical grade, with a viscosity of 15–25 cP, 1% in H_2O) were obtained from Sigma-Aldrich (Shanghai, China). 1-ethyl-3(3-(dimethylamino)propyl) carbodiimide (EDC) and N-hydroxysuccinimide (NHS) were purchased from Sigma-Aldrich. All of the other chemicals were at least of analytical grade and used as-received without further purification. L929 cells were obtained from the Institute of Biochemistry and Cell Biology (The Chinese Academy of Sciences, Shanghai, China). Dulbecco's Modified Eagle's Medium (DMEM), fetal bovine serum (FBS), glutaraldehyde, and MTT were purchased from Shanghai Limin Industrial Co., Ltd. (Shanghai, China). Water used in all of the experiments was purified using a Milli-Q Plus 185 water-purification system (Millipore, Bedford, MA, USA) with a resistivity higher than 18.2 MΩ·cm.

Preparation Of Alg-CS-Flu Scaffold

CS was dissolved in 100 mL of acetic acid solution (1 wt. %) with an optimized concentration of 3% (w/v). The milli-Q water was used as the solvent for dissolving Alg at a concentration of 4%. Then, a certain amount of Alg solution was added to the above CS solution, followed by continuous stirring for 2 hrs to obtain a homogeneous solution mixed with Flu (4 wt.% relative to Alg/CS). Next, the sticky mixed solution was coated onto a Petri dish before simple ultrasonic de-aeration. Finally, the obtained composites were freeze-dried at −80°C for 48 hrs.

Then, 0.35 g of EDC and 0.15 g of NHS were dissolved in 100 mL of 95% ethanol and stirred for 30 mins to obtain a homogeneous solution of EDC/NHS crosslinking solution. The dried 3 cm × 3 cm strips of Alg/CS scaffolds were dispersed in the EDC/NHS crosslinking solution for 3 hrs and then washed in double-distilled water; the crosslinked Alg/CS scaffold was named the Alg-CS scaffold. At the same time, Flu (100 mg), EDC (20 mmol, 3.83 mg), and NHS (50 mmol, 5.79 mg) were dissolved in 2 mL of PBS each. Then, all three solutions were mixed and stirred for 5 h to activate Flu's carboxyl group. The Alg-CS scaffold was added into the above activated Flu solutions with stirring for 48 hrs. After 48 hrs of covalent reaction at room temperature, the scaffolds

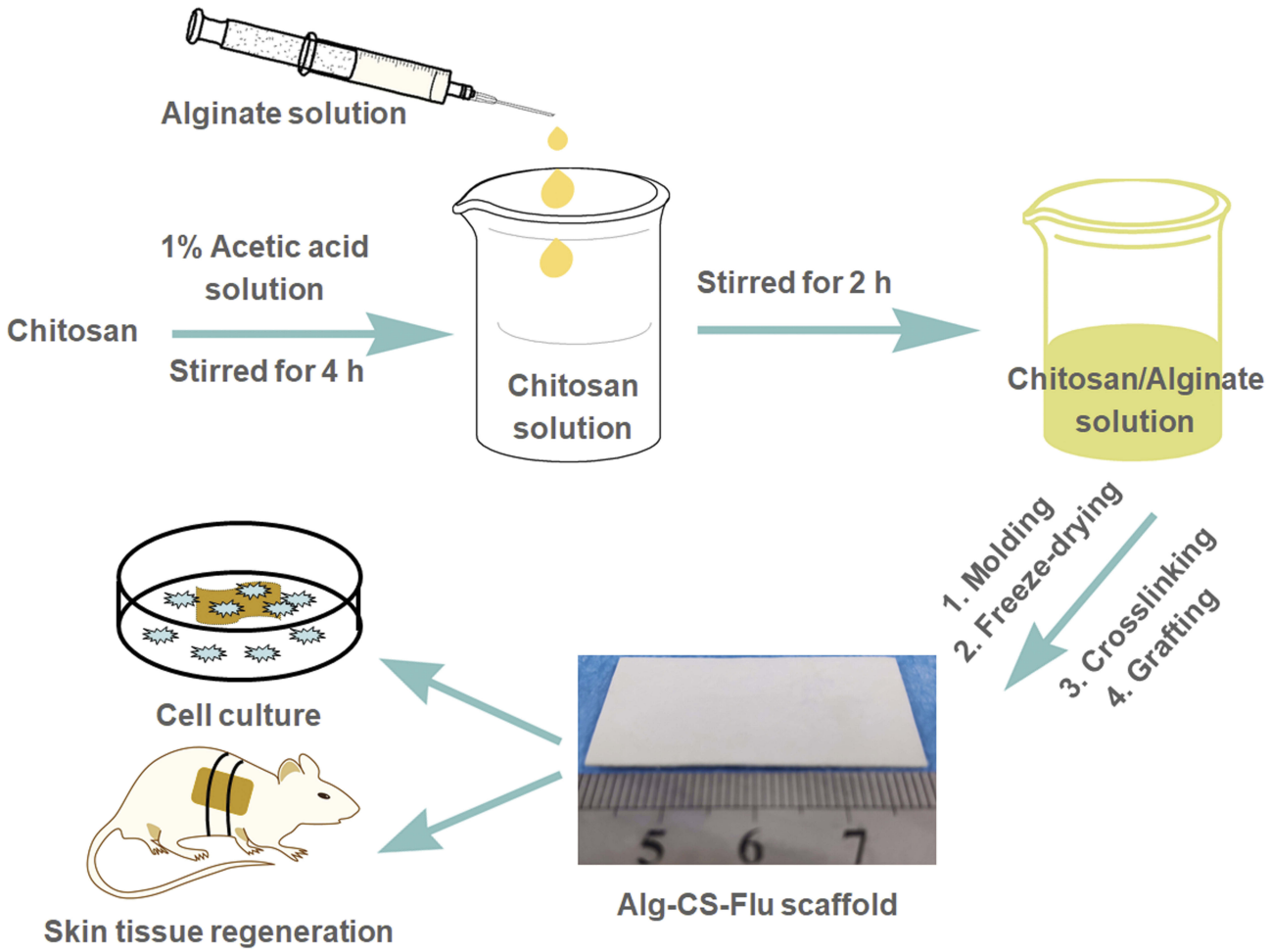

Figure 1 Schematic of preparation for fabrication of Alg-CS-Flu scaffolds.

were washed with copious amounts of Milli-Q water to remove the by-products, and then lyophilized for 48 hrs. The obtained Flu-grafted Alg-CS scaffolds were designated Alg-CS-Flu scaffolds.

Characterizations And Performance Testing

The morphology and structure of the as-prepared scaffolds were investigated by scanning electron microscopy (SEM) (Phenom, Phenom XL, Netherlands). The apparent water contact angle (WCA) was measured three times for each sample using a contact-angle instrument (OCA40, Data-physics, Germany) when the droplet was stable at 25°C±0.5°C and for a relative humidity of 30%±2%. Both WCA values of the right- and left-hand sides of the deionized water droplet were measured, and an average value was used. Wide-angle X-ray-diffraction (WAXRD) curves were obtained by a D/MAX-2550PC X-ray (Rigaku Inc., Tokyo, Japan) diffractometer with Cu *K*α radiation (*l*=1.5418 Å) at 45 kV and 40 mA, within the scanning region (2θ) of 5°–80°. The thermogravimetric analysis (TGA) of scaffolds was carried out using a TGA instrument (STA PT-1000, Linseis, Germany). A certain amount of sample (approximately 10 mg) was placed in a platinum pan and scanned from 25°C to 600°C at a heating rate of 20°C/min under a N_2 atmosphere, with a gas flow rate of 80 mL/min.[21–23]

The stress–strain curves, Young's modulus, and cyclic compression curves at 50% deformation of the scaffolds were tested in dry conditions by a tensile and cyclic tensile testing machine (HY-940FS, Shanghai Hengyu Instrument Co., Ltd, China). The tensile tests at a fixed rate of 0.2 mm/min and the cyclic tensile tests were repeated for 10 cycles at a fixed rate of 0.2 mm/min.

Cell Culture And Cytocompatibility Evaluation

The cytocompatibility of the ternary composite mat was assessed via MTT assay. In brief, coverslips and scaffolds

were fixed in 24-well plates with stainless-steel rings and sterilized by exposure to 75% alcohol solution for 2 hrs. After that, all of the samples were washed three times with PBS solution and soaked in DMEM overnight before cell seeding. Then, mouse fibroblast cells (L929) were seeded at a density of 1.5×10^4 cells per well for 2, 4, 8, and 12 hrs for cell adhesion assay and 1, 3, 5, and 7 d for cell proliferation assay. Coverslips without scaffolds were used as controls.

MTT assay and SEM observation were employed to separately evaluate the viability and morphology of the adhered and proliferated L929 cells cultured onto different scaffolds (n=3 for each group) according to the manufacturer's protocol of our previous research.[26] On a separate set of sheets, the attached cells were fixed with 4% paraformaldehyde and then 4′,6′-diamidino-2-phenylindole hydrochloride (DAPI, Invitrogen, USA) and fluorescein isothiocyanate-conjugated phalloidin (Invitrogen, USA) were used to stain the nucleus and cytoskeletons of cells. Specimens were observed under a TS100 fluorescence microscope (Nikon, Japan).

Subcutaneous Implantation In Mice And Histological Assessment

Six-week-old male mice (weighing approximately 180 g, purchased from Shanghai Jiesijie Laboratory Animal Co., Ltd, Shanghai, China) were chosen for subcutaneous implantation. A total of nine mice were used for this experiment, and they were divided into three groups for subcutaneous implantation for 7 d. Scaffolds sterilized with 75% ethanol vapor for 12 hrs were implanted symmetrically in two sides of the back of the same mouse. At a predetermined time point, the entire subcutaneous tissue containing scaffolds was excised from euthanized animals after 4 weeks of implantation and fixed in 4% (w/v) buffered formalin overnight. Samples were processed, sectioned to 300-μm thickness, and stained with hematoxylin and eosin (H&E) for histological analysis. The slides were observed using a light microscope (Olympus BX41, Japan) and photographed by a DP71 camera (Olympus, Japan).

Ethics Statement

The animal experimental protocols are in strict accordance with the policy of the Institutional Animal Care and Use Committee (IACUC) of Shanghai Jiao Tong University Affiliated Sixth People's Hospital. The IACUC has approved this study. The ethical principles were followed throughout all experiment procedures. All animal experiments were performed according to the Animal Management Regulations of China (1988 and revised in 2001, Ministry of Science and Technology).

Statistical Analysis

In all the experiments, at least three samples were performed and all results are represented as the mean ± standard deviation (SD). One-way ANOVA statistical method was used to evaluate the significance of the experimental data. A value of 0.05 was selected as the significance level, and the data were indicated with (*) for $p < 0.05$, (**) for $p < 0.01$, and (***) for $p < 0.001$, respectively.

Results And Discussion

Herein, a simple and effective strategy to regulate the preparation and construction of a functional Alg-CS scaffold with three-dimensional structure realized by facile freeze-drying combined with amidation is proposed. Figure 1 shows the fabrication process and formation mechanism of the functional scaffold with three-dimensional structure. CS with anti-inflammation, anti-bacterial, and wound-healing properties was purified from shrimp or crab shells. Alg and CS were crosslinked and numerous Flu molecules were grafted onto the surface of Alg-CS by amidation. The prepared Alg-CS-Flu is a kind of effectual scaffold for facilitating transdermal absorption or curing skin injury.

Characterization Of Scaffolds

The features of tissue engineering scaffolds, such as the diameter distribution of fibers and porosity, mean pore diameter, and surface hydrophilicity of scaffolds, are critical for tissue regeneration or repair processes.[27–29] According to our experimental design, the morphology and structural properties as well as the surface wettability of the surfaces of the as-prepared scaffolds were characterized by SEM and WCA (images of drops captured at 0.5 s) as presented in Figure 2. As can be seen from the SEM images in Figure 2(A and A′), the Alg/CS scaffold has a uniform porous and multi-layer structure and is a well-structured sponge-like material. The morphology of the Alg-CS scaffold as presented in Figure 2(B and B′), which was crosslinked with EDC/NHS, appeared macroscopically smooth, and the structures of the scaffold remain intact after the crosslinking process. In addition, the pore size becomes smaller compared with that of the Alg/CS scaffold. The Alg-CS-Flu scaffold was fabricated

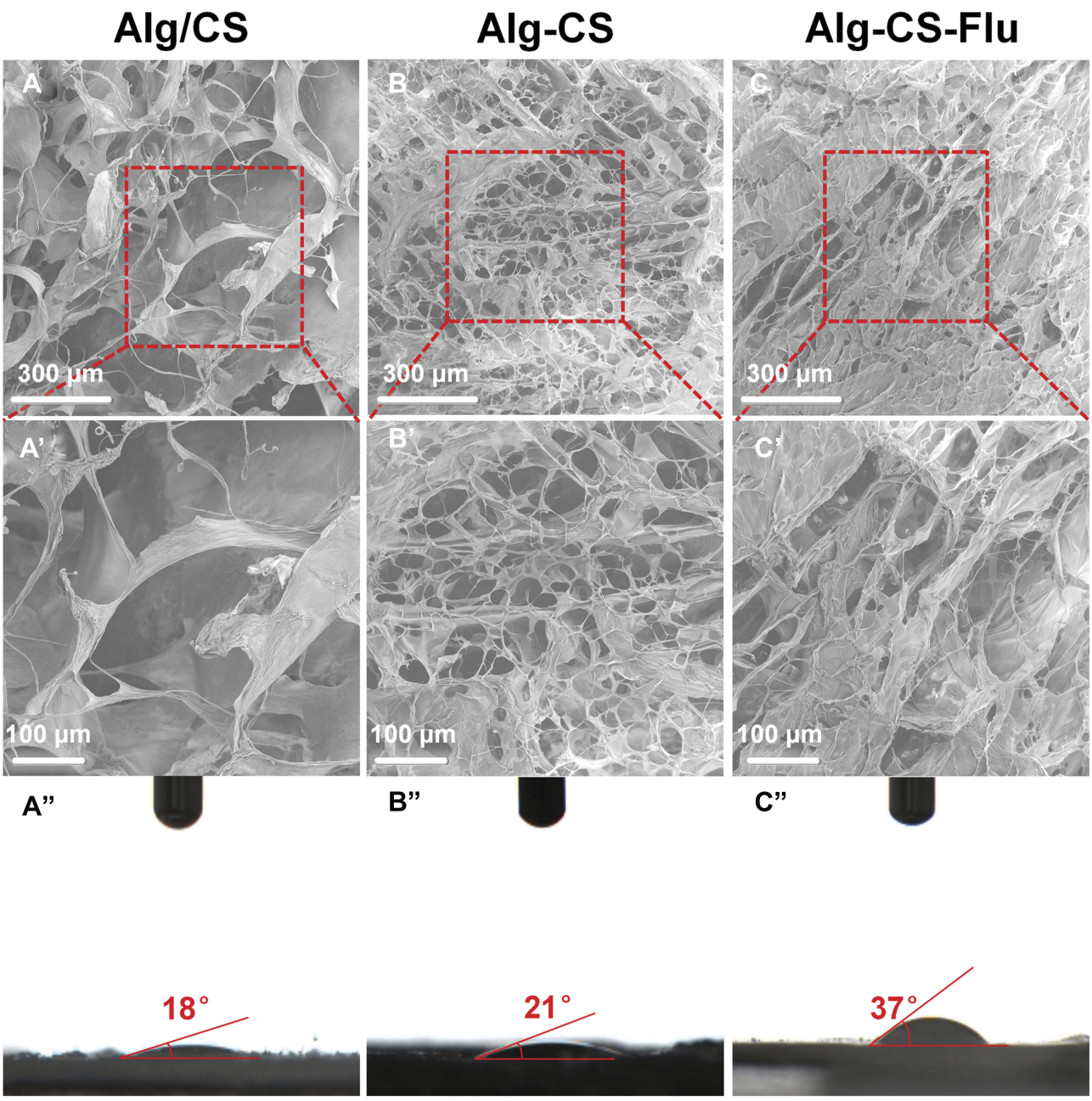

Figure 2 Surface SEM images and WCAs (images of drops captured at 0.5 s) of scaffolds: (**A**), (**A′**), and (**A″**) Alg/CS scaffold; (**B**), (**B′**), and (**B″**) Alg-CS scaffold; (**C**), (**C′**), and (**C″**) Alg-CS-Flu scaffold.

via two-step solution crosslinking modification. First, alginate with 1 mole of carboxyl in its molecular chain was crosslinked with 2 moles of amino chitosan via amidation. Then, the crosslinked scaffold was immersed in 1 mole of carboxyl Flu solution for chemical modification. The prepared Alg-CS-Flu scaffold possessed a denser three-dimensional structure. The smaller pore diameters of the Alg-CS-Flu scaffold compared to that of the Alg-CS scaffold were presumably due to the Flu molecules, which can be used as a crosslinking agent and possess short molecular chains and are easy to penetrate the three-dimensional bracket of the Alg-CS scaffold during grafting and freeze-drying.

Surface wettability of scaffolds greatly affects cell adhesion, proliferation, and migration.[30] The results of WCA measurements are exhibited in Figure 2(A″–C″). The Alg/CS scaffold showed its hydrophilic nature as the water drop stood well on its surface after it was dropped down, and its contact angle was measured to be approximately 18°. Regarding the Alg-CS and Alg-CS-Flu

scaffolds, their WCAs were increased due to the hydrophilic groups being used up after crosslinking. However, the WCA changed from 21° to 37° after Flu modification, which contributed to the denser three-dimensional structure of the Alg-CS-Flu scaffold.

Figure 3 shows the cross-sectional SEM images of the Alg/CS [Figure 3(A and A′)], Alg-CS [Figure 3(B and B′)], and Alg-CS-Flu scaffolds [Figure 3(C and C′)]. After the crosslinking process, the Alg-CS scaffold showed a compacted three-dimensional porous structure in its interior. Compared with the interior of the Alg-CS scaffold, the interior of the Alg-CS-Flu scaffold displayed a porous structure with appropriately sized pores (~80 μm) that allowed fast cell in-growth.

At present, most research focuses on the functionalization of CS/Alg composites that remain in blending or on the electrostatic interaction between carboxyl and primary amino groups.[14,21,31] In the present research, in contrast, two-step solution crosslinking modification was used to regulate the preparation of the three-dimensional porous scaffolds with the formation mechanisms shown in Figure 4. We can produce a stable three-dimensional scaffold by separately controlling the molar ratio of the carboxyl and amino groups of Alg, CS, and Flu.

In the development of composite materials for tissue engineering scaffolds, their amorphous or crystalline state and their compatibility are closely related to the molecular structure (Figure 5(A)) and are also vital for the materials' functional performances and stability of long-term preservation. The crystalline structural analysis of Alg/CS, Alg-CS, and Alg-CS-Flu composites was explored and is shown in Figure 5(B), in which the crystalline zones display sharp diffraction peaks and the amorphous regions show broader diffraction peaks. Alg/CS is composed of alginate and chitosan, which both are crystal materials, as demonstrated by two sharp Bragg reflections in its WAXRD pattern. For Alg/CS, the formation of amide bonds of Alg and CS molecular chains during the crosslinking process also affects the crystallization.[32] After crosslinking, the different peaks at 2θ=13° and 21.5°

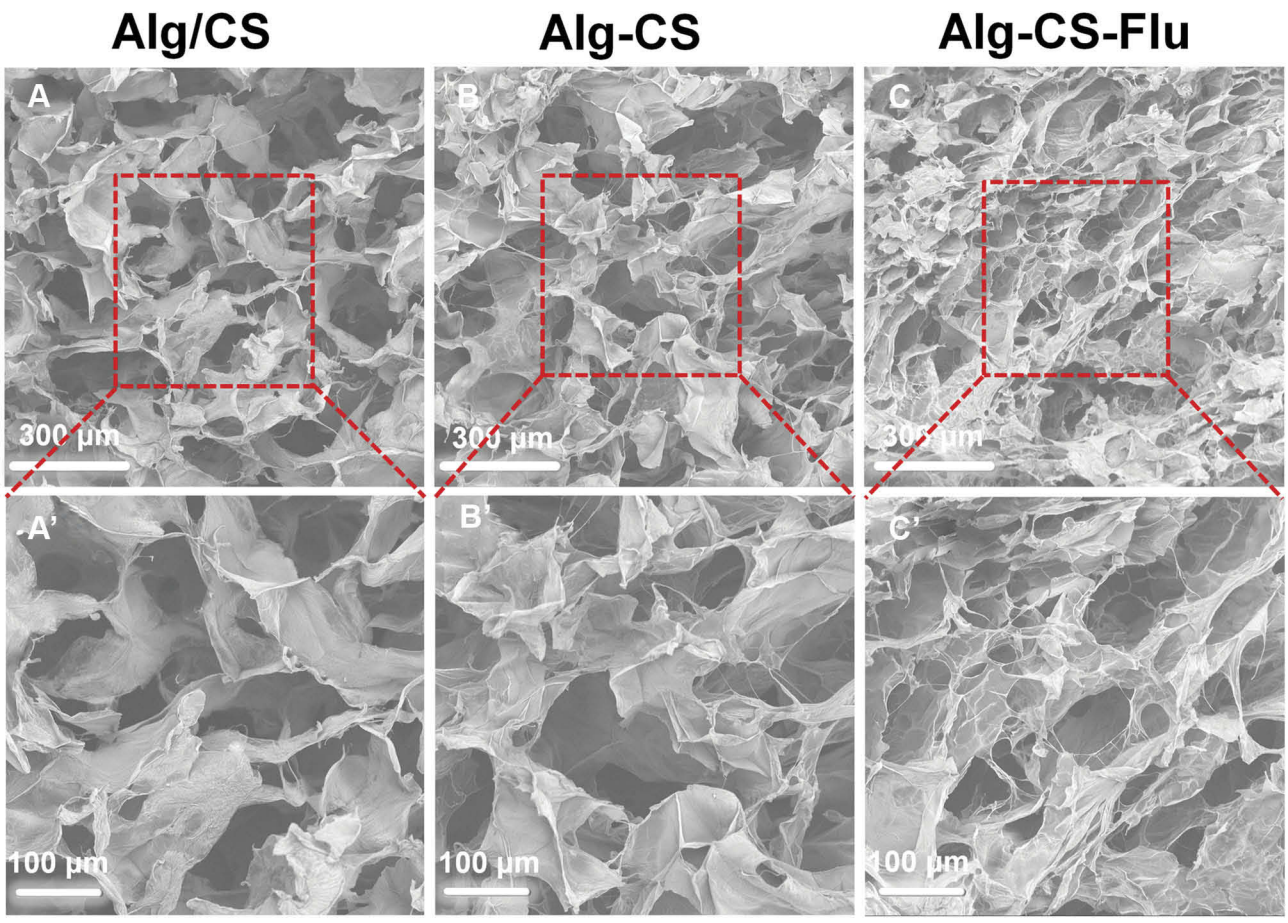

Figure 3 Cross-sectional SEM images of scaffolds: (**A** and **A′**) Alg/CS scaffold; (**B** and **B′**) Alg-CS scaffold; (**C** and **C′**) Alg-CS-Flu scaffold.

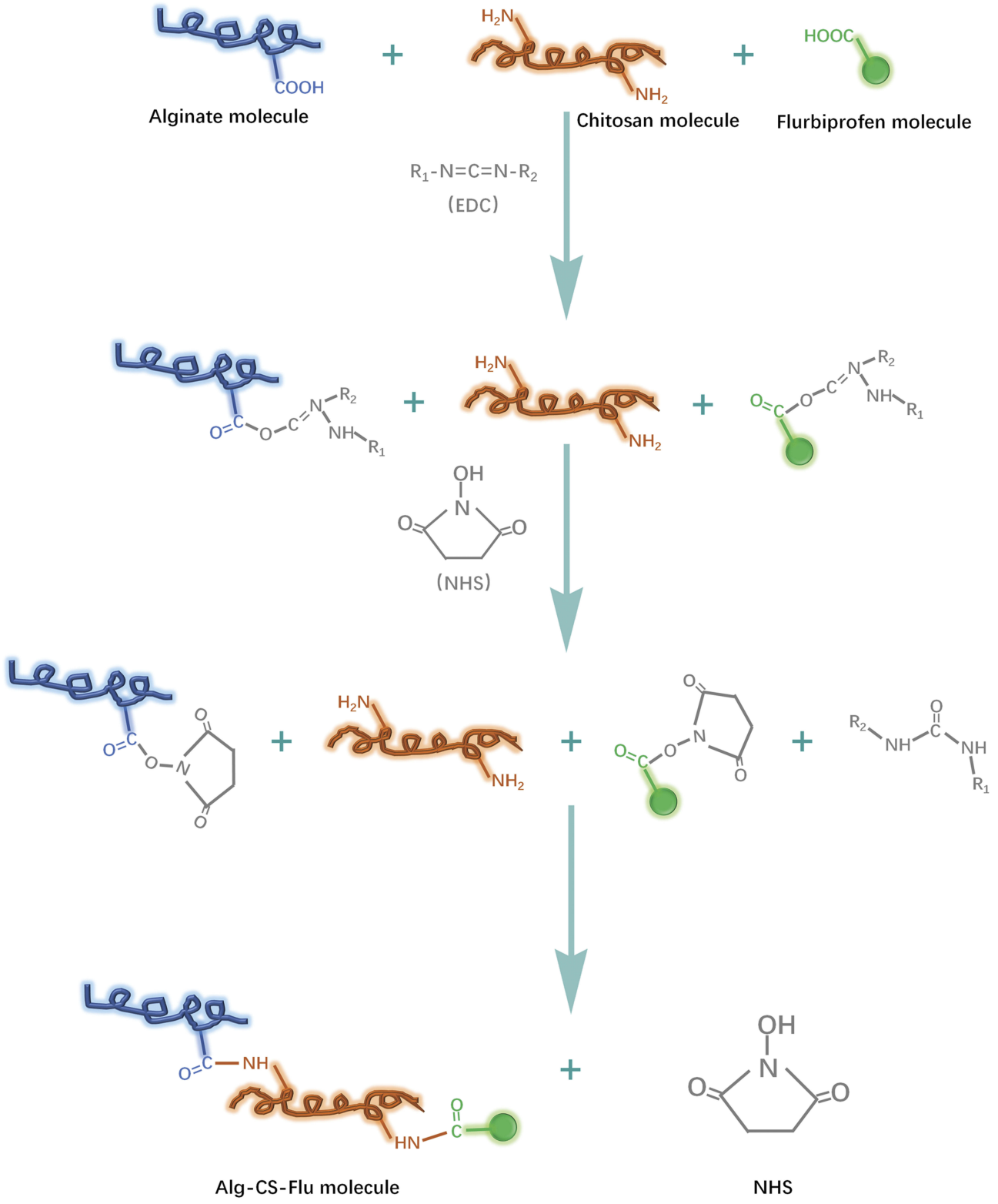

Figure 4 Formation mechanisms of Alg-CS-Flu molecule: crosslinking and grafting with EDC/NHS solution.

become diffuse, which is probably due to the molecular chain slips during the amidation reaction, and the intermolecular crystal structure has been destroyed. Comparing the different peaks of Alg-CS, the absorption peak in the crystal region of Alg-CS-Flu is weaker, which we believe to be due to the smaller Flu molecules being more likely to

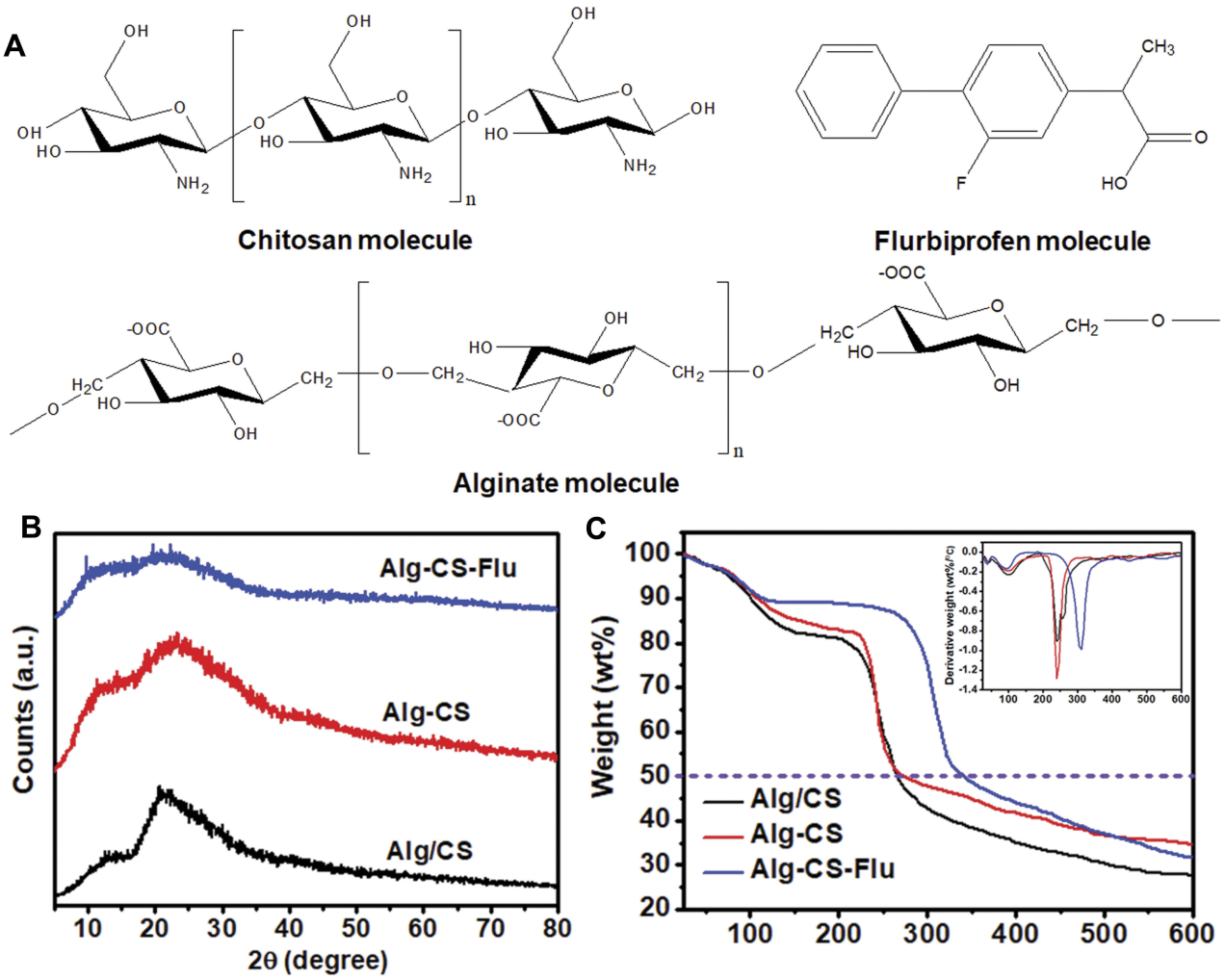

Figure 5 (**A**) Molecules of CS, Alg, and Flu; (**B**) WAXRD patterns of Alg/CS, Alg-CS, and Alg-CS-Flu scaffolds; (**C**) TG curves of Alg/CS, Alg-CS, and Alg-CS-Flu scaffolds; inset shows the DTG curves of scaffolds.

move in Alg and CS molecular chains, which makes it easier to destroy the original crystal structure of CS in the process of grafting.

Figure 5(C) shows the thermal degradation behavior of the prepared Alg-CS-Flu scaffold, compared with Alg/CS and Alg-CS. The pyrolytic process of the Alg/CS scaffold occurs in three stages: the dehydration of polymers, the thermal fracture of main molecular chains for Alg, and the thermal fracture of main molecular chains for CS and thermal scission of side chains (active groups: amino or carboxyl).[33] A moderate decrease in weight before 100°C could be due to the vaporization of water in the scaffolds. It can be seen that the onset temperatures of thermal degradation of Alg/CS and Alg-CS are between 110°C and 150°C, and the thermal degradation temperatures of Alg/CS and Alg-CS are near 270°C [can also be obtained from derivative thermogravimetry (DTG) curves in the inset of Figure 5(C)]. In Figure 5(C), the curves of the Alg-CS and Alg-CS-Flu scaffolds exhibit three stages: the dehydration of polymers, the thermal fracture of main molecular chains, and thermal scission of side chains. It can be observed that first weight loss at 40ºC–100ºC may be due to loss of water by evaporation. In addition, the thermal degradation temperature of the Alg-CS-Flu scaffold increased slightly. This may be due to the interaction between active groups (C=O and -OH) and the consequent formation of a tight entanglement of molecular chains.

Mechanical Properties

Mechanically matched scaffolds are essential for tissue engineering and regeneration. A mechanical mismatch between scaffold and host tissue would trigger foreign-body reactions and/or cause implantation failure.[34,35] Representative tensile stress–strain curves and the Young's moduli of Alg/CS, Alg-CS, and Alg-CS-Flu scaffolds are displayed in Figure 6(A). It

can be seen from Figure 6(C) that the zone of breaks of scaffolds are all located in the middle of the sample strip, indicating that this fracture test is effective. Compared to the Alg/CS scaffold, the crosslinking process leads to an obvious increase of tensile strength and Young's modulus and to an obvious decrease of elongation at the break of the Alg-CS and Alg-CS-Flu scaffolds in dry states. After crosslinking by EDC/NHS and Flu grafting, the tensile strength was approximately 20 kPa, which was less than that of the Alg-CS scaffold. This may be due to the formation of strong hydrogen bonds between Alg and CS molecules.

To further evaluate the elasticity of the Alg/CS, Alg-CS, and Alg-CS-Flu scaffolds, cyclic stretching was executed with a fixed strain of 50% in dry conditions. All of the scaffolds showed a larger hysteresis loop in the first cycle, and then smaller hysteresis loops were shown in the next nine cycles (Figures 6(D–I)). For 50% deformation in a dry state, the strain loss of the Alg/CS scaffold was approximately 25% in the first cycle, while for the Alg-CS and Alg-CS-Flu scaffolds, it was approximately 30%. This is probably due to the dense molecular network structure that is formed during the crosslinking and grafting processes, which changes the hardness of the scaffolds.

Cytocompatibility Assay In Vitro

For further skin tissue engineering applications, it is important to ensure the biocompatibility of the developed Alg-CS-Flu scaffold. In vitro adhesion and proliferation measured by MTT assay of mouse fibroblast cells (L929) after 2, 4, 8, and 12 hrs and 1, 3, 5, and 7 d after being cultured on the surfaces of Alg/CS, Alg-CS, and Alg-CS-Flu scaffolds are shown in Figure 7(A and B). Adhesion values of all scaffolds were significantly higher than that of coverslip group, regardless of culture time. In Figure 7 (C), the nucleus and skeleton were stained blue with DAPI and red with fluorescein isothiocyanate-conjugated

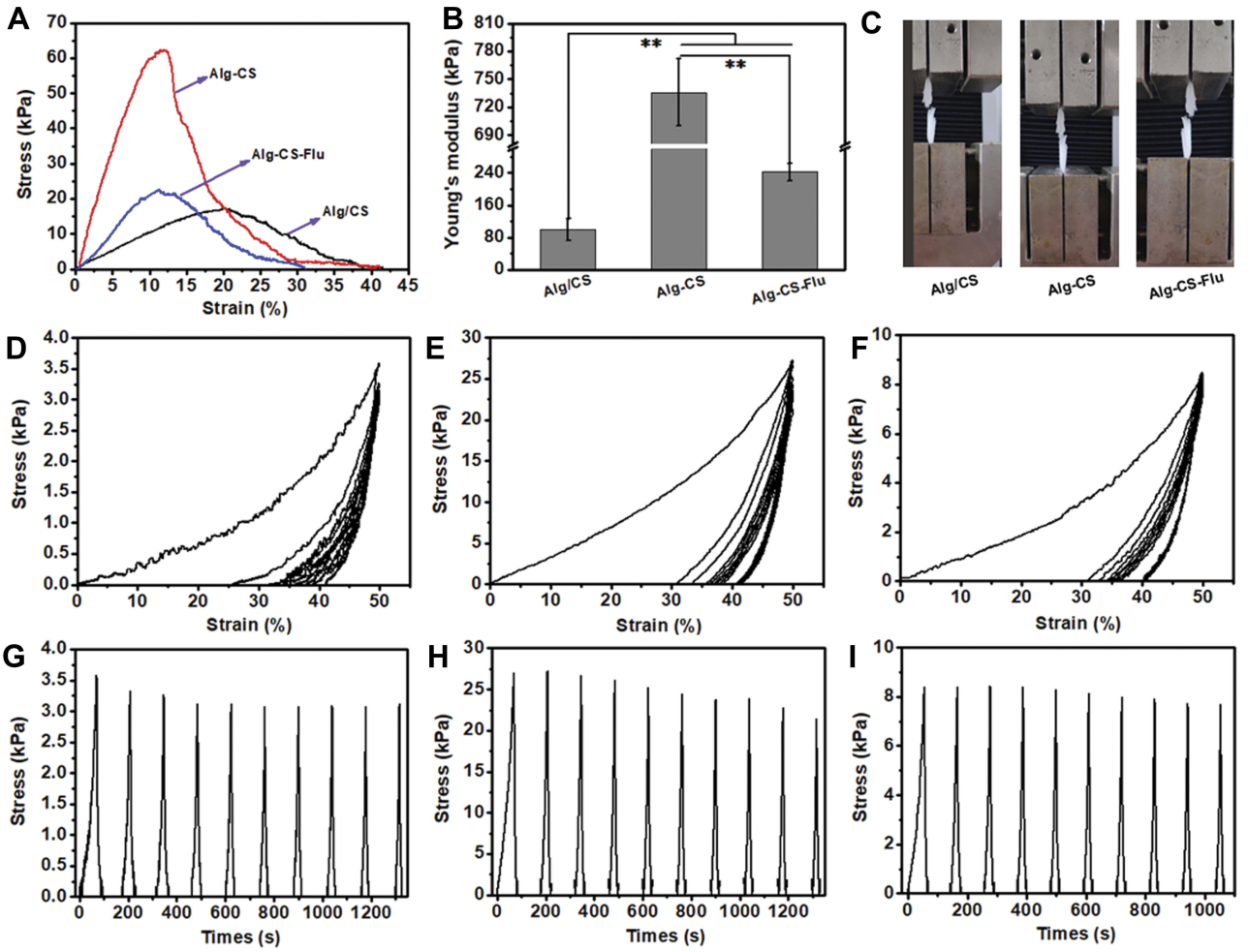

Figure 6 (**A**) Representative stress–strain curves; (**B**) Young's modulus; (**C**) photographs of fracture of scaffold strips; cyclic tensile response curves at 50% deformation of (**D**) and (**G**), Alg/CS scaffold, (**E**) and (**H**) Alg-CS scaffold, and (**F**) and (**I**) Alg-CS-Flu scaffold in dry states. **indicates significant difference at $p<0.01$ level.

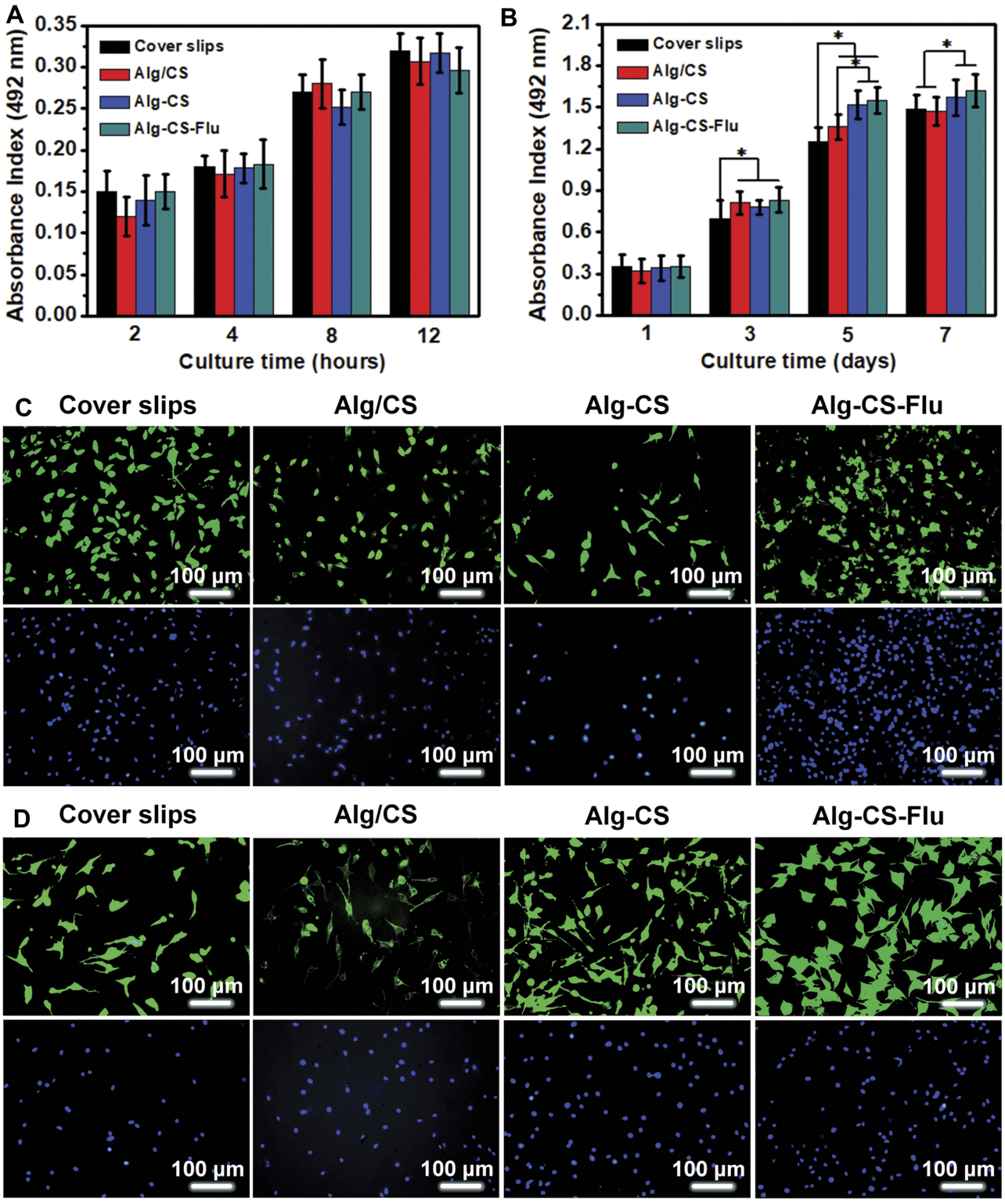

Figure 7 Adhesion viability and proliferation viability of L929 cells after culturing for (**A**) 12 hrs and (**B**) 7 d via MTT assay; (**C**) and (**D**) DAPI (blue)/rhodamine-conjugated phalloidin (red) staining assay of L929 cells on different scaffolds after culturing for 12 hrs and 5 d, respectively. *p<0.05.

phalloidin, respectively. From the fluorescence microscopy staining images for 12 h of L929 adhesion, the cells have a similar shape, and the cells on the surfaces of Alg-CS-Flu scaffold are spread more uniformly, as well as presenting more pseudopods. At day 1, there was no obvious difference among coverslips and scaffolds. However, at day 3,

scaffolds were more excellent in cell viability and showed a significant difference compared with coverslips (*p<0.05). When cultured after 5 d, the amount of cells exhibited a great increase, indicating that the Alg-CS-Flu scaffold enhanced cell growth and proliferation. Meanwhile, from day 7, as shown in Figure 7(B), the cell amount does not exhibit a more significant increase than that from day 5 and the Alg-CS-Flu scaffold was statistically significant (*p<0.05) compared with the Alg/CS scaffold and coverslips, because the three-dimensional porous structure of the Alg-CS-Flu scaffold is similar to the skeleton of the extracellular matrix, which is suitable for cell growth (Figure 7(d)). This is also evident from SEM micrographs of the Alg-CS-Flu scaffold exhibiting uniform porosity in Figures 2 and 3, which is the prerequisite for the proliferation of cells over the scaffold material.

It can be seen from the cell SEM results in Figure 8 that the L929 cells were tightly deposited onto the surfaces of scaffolds at 5 d. Compared to the coverslip group, the cell shapes of the scaffold groups tend to be multi-directional, rather than having a round shape. Moreover, the L929 cells were connected to each other and completely covered the surface of the Alg-CS-Flu scaffold. These cell morphology observation data corroborate the results of MTT assay.

Histological Evaluation Of Explanted Scaffolds In A Mouse Subcutaneous Model

Subcutaneous implantation (implanted in the back of 5-week-old male mice) to assess the in vivo biocompatibility of the Alg-CS-Flu. In the H&E staining images of scaffolds embedded into the subcutaneous tissue of the mice after 7 d, the nuclei evidenced a purple-blue color and the cytoplasm a red color. Moreover, the nuclei were presented regularly ovoid as well as the nucleoli were large and distinct. Therefore, we believe that these cells are inflammatory cells. As shown by the images in Figure 9, the inflammatory cells on the Alg-CS-Flu scaffold were significantly fewer than those on the Alg/CS and Alg-CS scaffolds. This subcutaneous implantation shows that the three-dimensional porous Alg-CS-Flu scaffold possesses a good anti-inflammatory property and histocompatibility.

Conclusion

In this study, we developed an Alg-CS-Flu scaffold via a facile freeze-drying technique combined with amidation. The experimental results indicate that a scaffold with a uniform three-dimensional pore structure was successfully fabricated. Furthermore, the prepared scaffold had desirable mechanical properties, as well as a sufficient modulus for skin tissue engineering applications. More importantly, the synergistic

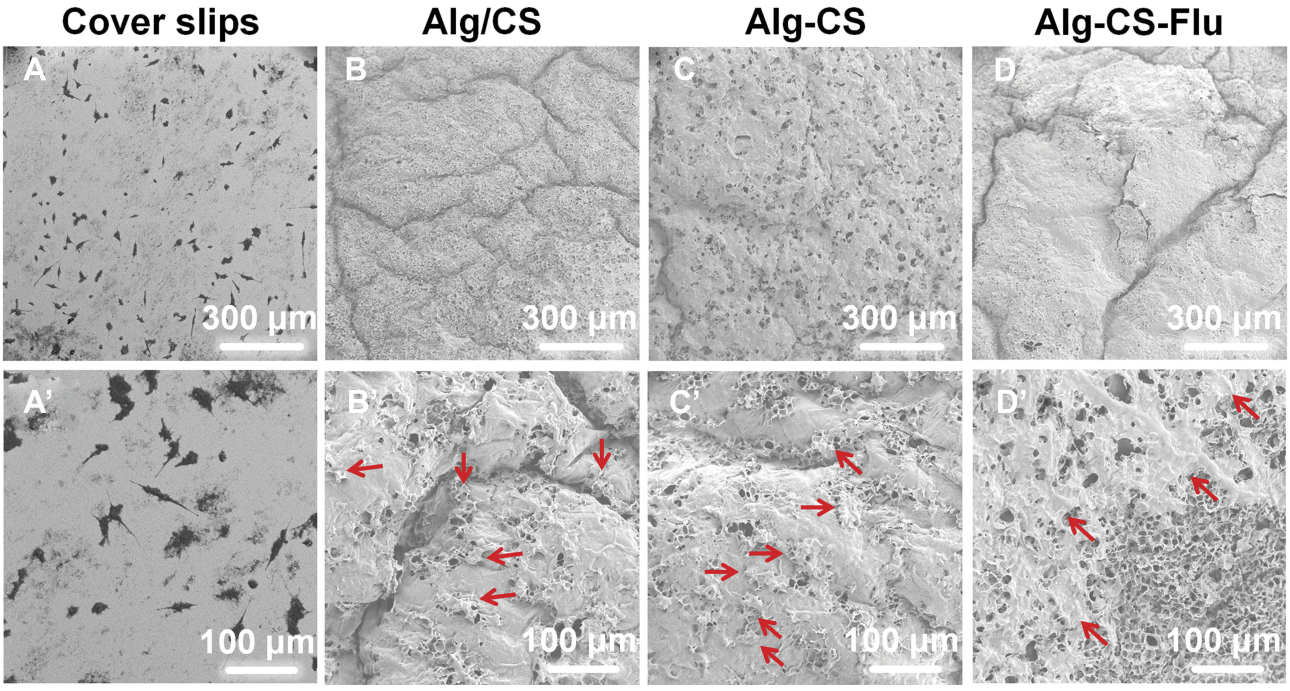

Figure 8 SEM micrographs of L929 cells grown onto (**A** and **A'**) coverslips; (**B** and **B'**) Alg/CS scaffold; (**C** and **C'**) Alg-CS scaffold; (**D** and **D'**) Alg-CS-Flu scaffold after 5-d culture. (**A**–**D**) magnified 200 times; (**A'**–**D'**) magnified 500 times. The red arrows represent L929 cells.

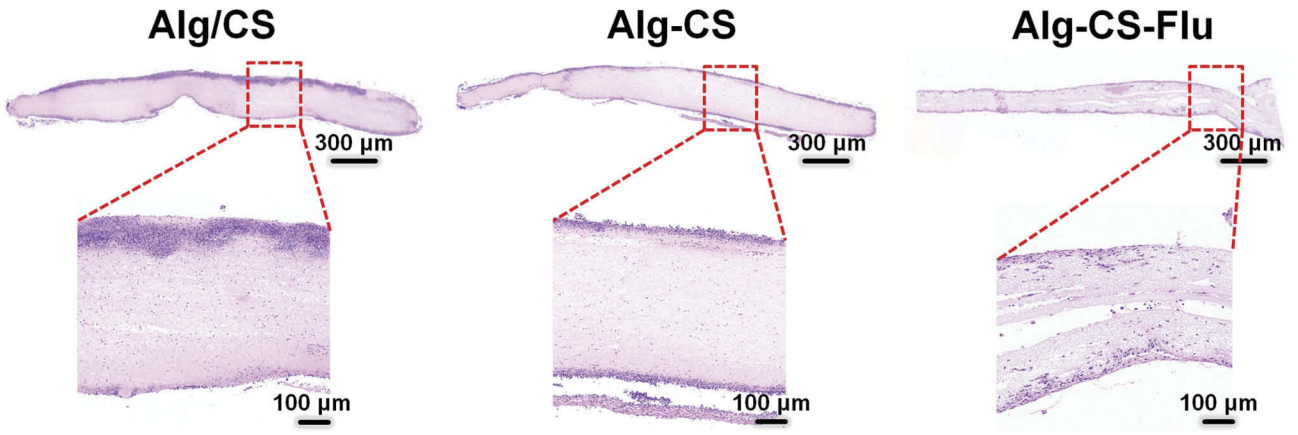

Figure 9 H&E staining images of transplanted Alg/CS, Alg-CS, and Alg-CS-Flu scaffolds after subcutaneous embedding in mice for 7 d.

effect of the grafted flurbiprofen and three-dimensional structure of the scaffold enhanced L929 cell adhesion and proliferation. The results of subcutaneous implantation tests show that the Alg-CS-Flu scaffold has a good anti-inflammatory property and histocompatibility as a result of being modified by flurbiprofen. This work outlines an effective way to promote rapid growth and migration of skin cells and to limit local inflammation.

Acknowledgment

The authors sincerely appreciate the supports of National Natural Science Foundation (Grant Nos. 81671920, 81871753, 81772341), National Key Research and Development Program of China (Grant Nos. 2018YFC 1106200, 2018YFC1106202), The Collaborative Innovation Transformation Project of Shanghai Jiao Tong University School of Medicine (Grant No. TM201736), The Project of Shenkang Hospital Development Center of Shanghai (Grant No. 16CR3108B), and The Technology Support Project of Science and Technology Commission of Shanghai Municipality of China (Grant No. 18441902800).

Disclosure

The authors report no conflicts of interest in this work.

References

1. Yu JR, Navarro J, Coburn JC, et al. Current and future perspectives on skin tissue engineering: key features of biomedical research, translational assessment, and clinical application. *Adv Healthc Mater*. 2019;8:5. doi:10.1002/adhm.201801471
2. John S, Kesting MR, Paulitschke P, Stockelhuber M, von Bomhard A. Development of a tissue-engineered skin substitute on a base of human amniotic membrane. *J Tissue Eng*. 2019;10:2041731418825378. doi:10.1177/2041731418825378
3. Shi QY, Luo X, Huang ZQ, et al. Cobalt-mediated multi-functional dressings promote bacteria-infected wound healing. *Acta Biomater*. 2019;86:465–479. doi:10.1016/j.actbio.2018.12.048
4. Ran LX, Zou YN, Cheng JW, Lu F. Silver nanoparticles in situ synthesized by polysaccharides from Sanghuangporus sanghuang and composites with chitosan to prepare scaffolds for the regeneration of infected full-thickness skin defects. *Int J Biol Macromol*. 2019;125:392–403. doi:10.1016/j.ijbiomac.2018.12.052
5. Ren XZ, Han YM, Wang J, et al. An aligned porous electrospun fibrous membrane with controlled drug delivery-An efficient strategy to accelerate diabetic wound healing with improved angiogenesis. *Acta Biomater*. 2018;70:140–153. doi:10.1016/j.actbio.2018.02.010
6. Giuri D, Barbalinardo M, Sotgiu G, et al. Nano-hybrid electrospun non-woven mats made of wool keratin and hydrotalcites as potential bio-active wound dressings. *Nanoscale*. 2019. doi:10.1039/c8nr10114k
7. Gao ST, Tang GS, Hua DW, et al. Stimuli-responsive bio-based polymeric systems and their applications. *J Mater Chem B*. 2019;7:709–729. doi:10.1039/C8TB02491J
8. Sun LM, Li AP, Hu YZ, Li Y, Shang L, Zhang LB. Self-assembled fluorescent and antibacterial GHK-Cu nanoparticles for wound healing applications. *Part Part Syst Charact*. 2019;1800420. doi:10.1002/ppsc.201800420
9. Ding QQ, Xu XW, Yue YY, et al. Nanocellulose-mediated electroconductive self-healing hydrogels with high strength, plasticity, viscoelasticity, stretchability, and biocompatibility toward multifunctional applications. *ACS Appl Mater Inter*. 2018;10(33):27987–28002. doi:10.1021/acsami.8b09656
10. Ren HH, Cui Y, Li AL, Qiu D. Bioactive glass sol as a dual function additive for chitosan-alginate hybrid scaffold. *Chinese Chem Lett*. 2018;29:395–398. doi:10.1016/j.cclet.2018.01.023
11. Tan Q, Tang H, Hu JG, et al. Controlled release of chitosan/heparin nanoparticle delivered VEGF enhances regeneration of decellularized tissue-engineered scaffolds. *Int J Nanomed*. 2011;6:929–942. doi:10.2147/IJN.S18753
12. Del Bakhshayesh AR, Annabi N, Khalilov R, et al. Recent advances on biomedical applications of scaffolds in wound healing and dermal tissue engineering. *Artif Cell Nanomed B*. 2018;46(4):691–705. doi:10.1080/21691401.2017.1349778
13. Mei L, Fan RR, Li XL, et al. Nanofibers for improving the wound repair process: the combination of a grafted chitosan and an antioxidant agent. *Polym Chem*. 2017;8(10):1664–1671. doi:10.1039/C7PY00038C

14. Kong Y, Xu R, Darabi MA, et al. Fast and safe fabrication of a free-standing chitosan/alginate nanomembrane to promote stem cell delivery and wound healing. *Int J Nanomed*. 2016;11:2543–2555.
15. Rubio-Elizalde I, Bernaldez-Sarabia J, Moreno-Ulloa A, et al. Scaffolds based on alginate-PEG methyl ether methacrylate-Moringa oleifera-Aloe vera for wound healing applications. *Carbohyd Polym*. 2019;206:455–467. doi:10.1016/j.carbpol.2018.11.027
16. Mao W, Kang MK, Shin JU, Son YJ, Kim HS, Yoo HS. Coaxial hydro-nanofibrils for self-assembly of cell sheets producing skin bilayers. *ACS Appl Mater Inter*. 2018;10(50):43503–43511. doi:10.1021/acsami.8b17740
17. Penhasi A, Reuveni A. Preparation and evaluation of a bio-erodible bio-adhesive drug delivery system designed for intraoral extended release of flurbiprofen: in vitro and in vivo assessments. *J Pharm Innov*. 2019;14(1):15–27. doi:10.1007/s12247-018-9327-z
18. Isola G, Alibrandi A, Pedulla E, et al. Analysis of the effectiveness of lornoxicam and flurbiprofen on management of pain and sequelae following third molar surgery: a randomized, controlled, clinical trial. *J Clin Med*. 2019;8(3). doi:10.3390/jcm8030325
19. Zhu TH, Chen SH, Li WY, Lou JZ, Wang JH. Flurbiprofen axetil loaded coaxial electrospun poly(vinyl pyrrolidone)-nanopoly(lactic-co-glycolic acid) core-shell composite nanofibers: preparation, characterization, and anti-adhesion activity. *J Appl Polym Sci*. 2015;132 (22). doi:10.1002/APP.41982
20. Shinde UA, Joshi PN, Jain DD, Singh K. Preparation and evaluation of N-trimethyl chitosan nanoparticles of flurbiprofen for ocular delivery. *Cuee Eye Res*. 2019. doi:10.1080/02713683.2019.1567793
21. Chen Y, Qiu HY, Dong MH, et al. Preparation of hydroxylated lecithin complexed iodine/carboxymethyl chitosan/sodium alginate composite membrane by microwave drying and its applications in infected burn wound treatment. *Carbohyd Polym*. 2019;206:435–445. doi:10.1016/j.carbpol.2018.10.068
22. Li KJ, Zhu JX, Guan GL, Wu H. Preparation of chitosan-sodium alginate films through layer-by-layer assembly and ferulic acid crosslinking: film properties, characterization, and formation mechanism. *Int J Biol Macromol*. 2019;122:485–492. doi:10.1016/j.ijbiomac.2018.10.188
23. Denkbas EB, Ozturk E, Ozdemir N, Kececi K, Ergun MA. EGF loaded chitosan sponges as wound dressing material. *J Bioact Compat Pol*. 2003;18(3):177–190. doi:10.1177/0883911503035388
24. Zeng HY, Huang YC. Basic fibroblast growth factor released from fucoidan-modified chitosan/alginate scaffolds for promoting fibroblasts migration. *J Polym Res*. 2018;25(3). doi:10.1007/s10965-018-1476-8
25. Che AF, Liu ZM, Huang XJ, Wang ZG, Xu ZK. Chitosan-modified poly(acrylonitrile-co-acrylic acid) nanofibrous membranes for the immobilization of concanavalin A. *Biomacromolecules*. 2008;9 (12):3397–3403. doi:10.1021/bm800882z
26. Zhu TH, Yu K, Bhutto MA, et al. Synthesis of RGD-peptide modified poly(ester-urethane) urea electrospun nanofibers as a potential application for vascular tissue engineering. *Chem Eng J*. 2017;315:177–190. doi:10.1016/j.cej.2016.12.134
27. Ding JX, Zhang J, Li JN, et al. Electrospun polymer biomaterials. *Prog Polym Sci*. 2019;90:1–34. doi:10.1016/j.progpolymsci.2019.01.002
28. Wei DX, Dao JW, Chen GQ. A micro-ark for cells: highly open porous polyhydroxyalkanoate microspheres as injectable scaffolds for tissue regeneration. *Adv Mater*. 2018;30(31). doi:10.1002/adma.201802273
29. Deng AP, Yang Y, Du SM, Yang SL. Electrospinning of in situ crosslinked recombinant human collagen peptide/chitosan nanofibers for wound healing. *Biomater Sci*. 2018;6(8):2197–2208. doi:10.1039/C8BM00492G
30. Menon NV, Chuah YJ, Phey S, et al. Microfluidic assay to study the combinatorial impact of substrate properties on mesenchymal stem cell migration. *ACS Appl Mater Inter*. 2015;7(31):17095–17103. doi:10.1021/acsami.5b03753
31. Wang HP, Gong XC, Miao YL, et al. Preparation and characterization of multilayer films composed of chitosan, sodium alginate and carboxymethyl chitosan-ZnO nanoparticles. *Food Chem*. 2019;283:397–403. doi:10.1016/j.foodchem.2019.01.022
32. Shameli K, Ahmad MB, Zargar M, et al. Synthesis and characterization of silver/montmorillonite/chitosan bionanocomposites by chemical reduction method and their antibacterial activity. *Int J Nanomed*. 2011;6:271–284. doi:10.2147/IJN.S16043
33. Carneiro-da-Cunha MG, Cerqueira MA, Souza BWS, et al. Physical and thermal properties of a chitosan/alginate nanolayered PET film. *Carbohyd Polym*. 2010;82(1):153–159. doi:10.1016/j.carbpol.2010.04.043
34. Baruch L, Machluf M. Alginate-chitosan complex coacervation for cell encapsulation: effect on mechanical properties and on long-term viability. *Biopolymers*. 2006;82(6):570–579. doi:10.1002/(ISSN)1097-0282
35. Ramay HR, Li ZS, Shum E, Zhang MQ. Chitosan-alginate porous scaffolds reinforced by hydroxyapatite nano- and micro-particles: structural, mechanical, and biological properties. *J Biomed Nanotechnol*. 2005;1(2):151–160. doi:10.1166/jbn.2005.026